Article

TRANSPARENT PROCESS

THE EMBO JOURNAL

A postprandial FGF19-SHP-LSD1 regulatory axis mediates epigenetic repression of hepatic autophagy

Sangwon Byun[1], Young-Chae Kim[1], Yang Zhang[2], Bo Kong[3], Grace Guo[3], Junichi Sadoshima[4], Jian Ma[2,5], Byron Kemper[1] & Jongsook Kim Kemper[1,*]

Abstract

Lysosome-mediated autophagy is essential for cellular survival and homeostasis upon nutrient deprivation, but is repressed after feeding. Despite the emerging importance of transcriptional regulation of autophagy by nutrient-sensing factors, the role for epigenetic control is largely unexplored. Here, we show that Small Heterodimer Partner (SHP) mediates postprandial epigenetic repression of hepatic autophagy by recruiting histone demethylase LSD1 in response to a late fed-state hormone, FGF19 (hFGF19, mFGF15). FGF19 treatment or feeding inhibits macroautophagy, including lipophagy, but these effects are blunted in SHP-null mice or LSD1-depleted mice. In addition, feeding-mediated autophagy inhibition is attenuated in FGF15-null mice. Upon FGF19 treatment or feeding, SHP recruits LSD1 to CREB-bound autophagy genes, including Tfeb, resulting in dissociation of CRTC2, LSD1-mediated demethylation of gene-activation histone marks H3K4-me2/3, and subsequent accumulation of repressive histone modifications. Both FXR and SHP inhibit hepatic autophagy interdependently, but while FXR acts early, SHP acts relatively late after feeding, which effectively sustains postprandial inhibition of autophagy. This study demonstrates that the FGF19-SHP-LSD1 axis maintains homeostasis by suppressing unnecessary autophagic breakdown of cellular components, including lipids, under nutrient-rich postprandial conditions.

Keywords bile acid; CREB; CRTC2; FGF15; FXR; lipophagy; TFEB
Subject Categories Autophagy & Cell Death; Chromatin, Epigenetics, Genomics & Functional Genomics; Metabolism
DOI 10.15252/embj.201695500 | Received 15 August 2016 | Revised 31 March 2017 | Accepted 4 April 2017 | Published online 26 April 2017
The EMBO Journal (2017) 36: 1755–1769

Introduction

Lysosome-mediated autophagy is a highly conserved homeostatic process that recycles cellular components and mobilizes energy stores, including lipid droplets, in response to nutrient deprivation (Klionsky, 2007; Mizushima, 2009; Singh *et al*, 2009; Rabinowitz & White, 2010; Singh & Cuervo, 2012). Autophagy is known to occur under extremely stressful starvation conditions, but increasing evidence indicates that it also occurs during feeding/fasting cycles under normal physiological conditions (Settembre *et al*, 2013; Lee *et al*, 2014; Seok *et al*, 2014). Autophagy is regulated acutely by nutrient-sensing cytoplasmic kinases, such as mTOR and AMPK (Egan *et al*, 2011; Kim *et al*, 2011), but recent studies demonstrate that nuclear events are also important for sustained autophagy regulation. Nutrient-sensing transcriptional factors, including fasting-activated CREB, PPARα, and TFEB, and feeding-activated FXR, dynamically activate or repress macroautophagy, including autophagy-mediated lipid breakdown, "lipophagy" (Settembre *et al*, 2013; Lee *et al*, 2014; Seok *et al*, 2014).

Epigenetic modifications, including histone modifications, play a crucial role in linking environmental cues, such as changes in metabolite levels, to regulation of gene expression to maintain homeostasis (Teperino *et al*, 2010; Lu & Thompson, 2012; Smith *et al*, 2012). Despite the emerging importance of transcriptional regulation in autophagy, only a few studies have examined epigenetic control of autophagy (Artal-Martinez de Narvajas *et al*, 2013; Fullgrabe *et al*, 2013; Shin *et al*, 2016), and its role in directly linking nutritional status to autophagy-mediated lipid degradation in animals *in vivo* has not been described.

An orphan nuclear receptor, Small Heterodimer Partner (SHP, NR0B2), is a key transcriptional regulator that links changes in hepatic bile acid levels to epigenetic repression of bile acid synthetic genes to maintaining bile acid homeostasis (Kerr *et al*, 2002; Wang *et al*, 2002; Smith *et al*, 2012; Kim *et al*, 2016). In response to elevated hepatic bile acid levels and bile acid-induced fibroblast

1 Department of Molecular and Integrative Physiology, University of Illinois at Urbana-Champaign, Urbana, IL, USA
2 Department of Bioengineering, University of Illinois at Urbana-Champaign, Urbana, IL, USA
3 Department of Pharmacology and Toxicology, Ernest Mario School of Pharmacy, Rutgers, The State University of New Jersey, Piscataway, NJ, USA
4 Department of Cell Biology and Molecular Medicine, Cardiovascular Research Institute, Rutgers New Jersey Medical School, Newark, NJ, USA
5 Computational Biology Department, School of Computer Science, Carnegie Mellon University, Pittsburgh, PA, USA
*Corresponding author. Tel: +1 217 333 6317; E-mail: jongsook@illinois.edu

growth factor-19 (hFGF19, mFGF15) signaling after feeding (Inagaki *et al*, 2005; Kir *et al*, 2011), SHP epigenetically represses transcription of bile acid synthetic genes, *Cyp7a1 and Cyp8b1,* by recruiting repressive histone-modifying enzymes, including LSD1 histone demethylase (Kemper *et al*, 2004; Fang *et al*, 2007; Kim *et al*, 2015b). Based on published ChIP-seq analysis of mice treated with a late fed-state hormone FGF19 (Kim *et al*, 2015a), SHP binding peaks were detected at over 80 autophagy-related genes in liver, suggesting a previously unrecognized role for SHP in epigenetic control of autophagy.

Here, we identify a new function of an FGF19-SHP-LSD1 axis in transcriptional and epigenetic repression of hepatic autophagy in the late fed-state. After treatment with FGF19 or feeding, SHP recruits LSD1 to a group of CREB-target autophagy-related genes, including *Tfeb,* resulting in disruption of the CREB-CRTC2 transactivation complex and an epigenetic cascade leading to gene repression. We further show that both feeding-sensing FXR and SHP inhibit autophagy in a mutually dependent manner, but FXR acts predominantly early after feeding, while SHP acts relatively late, which effectively sustains postprandial inhibition of autophagy.

Results

SHP inhibits hepatic autophagy *in vivo*

From liver ChIP-seq studies of FGF19-treated mice (Kim *et al*, 2015a), SHP binding peaks were detected within 10 kb of the transcription start sites (TSS) in 85 of the 230 autophagy-related genes in the Human Autophagy Database (http://autophagy.lu/) (Appendix Fig S1 and Appendix Table S1). In ChIP analyses, treatment with FGF19 increased SHP occupancy at all tested autophagy-related genes and a known SHP-target gene, *Cyp7a1* (Fig 1A), and decreased mRNA levels of most of these autophagy genes in WT mice (Fig 1B). In contrast, in $SHP^{-/-}$ mice, the basal expression of these genes was elevated and the inhibition by FGF19 was blunted (Fig 1B), suggesting that SHP is required for FGF19 inhibition of autophagy genes.

To determine whether FGF19 treatment inhibits hepatic autophagy, we examined the expression of LC3 and p62, markers of autophagy (Mizushima *et al*, 2010). Phosphatidylethanolamine-conjugated LC3-II is present on autophagosome membranes, and the ratio of LC3-II to LC3-I is an indicator of autophagic flux. Conversely, the autophagosome adaptor protein, p62/SQSTM1, is degraded by autophagy, and thus, p62 accumulates when autophagy is inhibited. We examined hepatic autophagy by immunohistochemistry (IHC) and immunofluorescence (IF). LC3-I appears diffuse in the cytoplasm and LC3-II appears as distinct puncta. FGF19 treatment decreased the number of endogenous LC3-II puncta (Fig 1C) or exogenous GFP-LC3-II puncta (Fig 1D) and increased p62 levels (Fig 1C) in WT mouse liver, whereas these changes were blunted in livers of $SHP^{-/-}$ mice. FGF19 signaling assessed by p-ERK levels (Kir *et al*, 2011) was normal in SHP-KO mice (Appendix Fig S2A). These results demonstrate that FGF19 inhibition of autophagy is SHP-dependent.

Nutrient-sensing mTOR complex 1 (mTORC1) was shown to negatively regulate autophagy by phosphorylation of ULK1 at S757 (Kim *et al*, 2011), so it is possible that FGF19 inhibition of autophagy is affected by mTOR signaling. To test this idea, we examined the effect of rapamycin, an allosteric inhibitor of mTORC1, FGF19, or both, on hepatic autophagy in mice. Treatment with rapamycin decreased p-S757-ULK1 levels and increased autophagic flux as assessed by the increased ratio of LC3-II to LC-I as expected (Appendix Fig S2B). FGF19 treatment inhibited autophagic flux without changing the levels of mTORC1 targets, p-S6K or p-ULK1, and co-treatment with rapamycin and FGF19 largely blunted the rapamycin-induced autophagic flux without changing the p-S757-ULK1 levels. FGF19 treatment also increased p-ERK levels as expected, whereas p-AMPK levels were not changed (Appendix Fig S2C). Further, in primary mouse hepatocytes, treatment with a lysosomal inhibitor, bafilomycin-A1, did not block the decreased ratio of LC3-II to LC-I after FGF19 treatment (Appendix Fig S2D). These results suggest that FGF19 inhibition of autophagy is likely independent of mTORC1 or lysosomal function.

SHP represses hepatic autophagy after feeding in an FGF15-dependent manner

FGF15/19 is a late fed-state hormone that is induced by the intestinal bile acid nuclear receptor FXR and acts at the liver to mediate postprandial metabolic responses independent of insulin action (Inagaki *et al*, 2005; Kir *et al*, 2011). Serum FGF15/19 levels peak about 3 h after feeding (Lundasen *et al*, 2006), which is considerably later than the peaks of insulin or bile acids.

To determine the physiological relevance of SHP-dependent FGF15/19 inhibition of autophagy, we next examined whether SHP is required for feeding-mediated inhibition of hepatic autophagy. Numbers of LC3-II puncta in liver were elevated in $SHP^{-/-}$ mice, the feeding-mediated decrease in the number of LC3-II puncta in WT mice was substantially attenuated in $SHP^{-/-}$ mice (Fig 1E and

Figure 1. SHP inhibits hepatic autophagy by FGF19 treatment or feeding.

A–D Mice were fasted for 12 h and injected via the tail vein with FGF19 (1 mg/kg) or vehicle for 2 h (A) or 6 h (B–D). (A) SHP occupancy in liver was detected by ChIP (n = 3), and (B) mRNA levels were detected by qRT–PCR (n = 6). (C) LC3 and p62 detected by IHC analysis of liver sections from WT or $SHP^{-/-}$ mice. Representative images of LC3-II puncta and quantitation are shown (n = 30 hepatocytes). (D) WT or $SHP^{-/-}$ mice were injected via the tail vein with Ad-GFP-LC3, and then, 1 week later the mice were treated with FGF19 or vehicle. Representative images of GFP-LC3-II puncta are shown.

E LC3 and p62 detected by IHC analysis of liver sections from fasted or fed WT or $SHP^{-/-}$ mice. Representative images of LC3-II puncta and quantitation are shown (n = 30 hepatocytes).

F Mice adenovirally expressing GFP-LC3 were fasted or fasted and refed, and representative images of GFP-LC3-II puncta in liver sections are shown.

G, H LC3 and p62 levels in liver extracts from fasted or fed WT or $SHP^{-/-}$ (G) or from fasted or fed WT or $FGF15^{-/-}$ (H) mice were measured by IB, and LC3-I and LC3-II intensities were quantified and the relative ratio of LC3-II to LC3-I was set to 1 for fasted WT mice (right, n = 3).

Data information: Means ± SD are shown, and statistical significance was measured using two-way ANOVA with the Bonferroni post-test. *P < 0.05, **P < 0.01, and NS, statistically not significant.

F), and the decreased ratio of LC3-II to LC3-I after feeding in WT mice was largely absent in $SHP^{-/-}$ mice (Fig 1G). Levels of p62 were reduced in $SHP^{-/-}$ mice and the increase in p62 after feeding in WT mice was not observed in $SHP^{-/-}$ mice (Fig 1E and G). Consistent with these results, mRNA levels of SHP-target autophagy genes were also decreased by feeding in WT, but not $SHP^{-/-}$ mice (Appendix Fig S3A). Importantly, feeding-mediated decreases in the LC3-II/LC3-I ratio (Fig 1H) and gene expression (Appendix Fig S3B) were largely abolished in $FGF15^{-/-}$ mice (Kong *et al*, 2014), indicating the dependence of SHP-mediated postprandial repression of

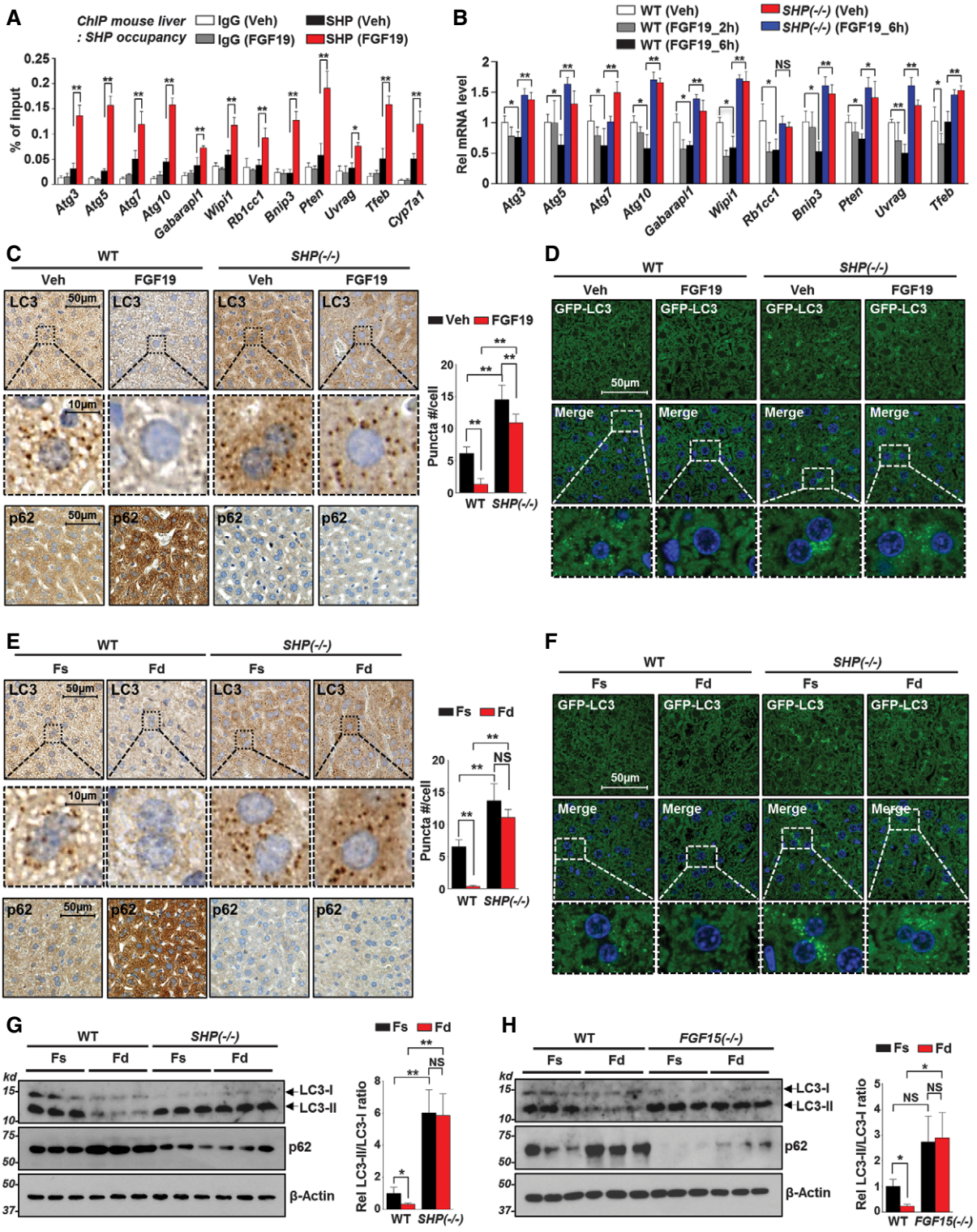

Figure 1.

hepatic autophagy on FGF15. These results demonstrate that SHP acts as a key physiological repressor of autophagy in response to FGF15/19 in the late fed-state.

SHP antagonizes the CREB transactivation of autophagy genes

To identify potential transcription factors that might recruit the non-DNA binding SHP to autophagy genes, we compared binding sites for the activators of autophagy, CREB (Everett *et al*, 2013), PPARα (Boergesen *et al*, 2012), and SREBP-2 (Seo *et al*, 2011) with those of SHP (Kim *et al*, 2015a) from published liver ChIP-seq data. CREB binding peaks overlapped with 63% of SHP binding peaks at autophagy genes, a substantially higher percentage than the overlap with PPARα and SREBP-2 (Fig 2A and Appendix Tables S2–S4), and one or more CREB binding motifs were present within the SHP binding regions (Appendix Table S5). We therefore focused on CREB, a master transcriptional activator that drives the fasting response (Herzig *et al*, 2001; Koo *et al*, 2005). Notably, nearly all of the binding peaks for SHP (Kim *et al*, 2015a) and CREB (Everett *et al*, 2013; Seok *et al*, 2014) were found within 1 kb of the TSS of autophagy-related genes (Appendix Table S2), including the key autophagy component genes *Atg3* and *Atg10*, and a key transcriptional activator of autophagy, *Tfeb* (Fig 2B). These results suggest that CREB may recruit SHP to autophagy-related genes.

After FGF19 treatment, occupancy of SHP at *Tfeb and Atg3* increased, that of the CREB coactivator CRTC2 decreased, and CREB occupancy was unaffected while no decrease in CRTC2 occupancy was observed in $SHP^{-/-}$ mice (Fig 2C). Similar results were observed for *Atg5, Atg10, and Pten* (Appendix Fig S4). These results suggest that the decreased occupancy of CRTC2 is dependent on SHP. Further, in re-CHIP assays, SHP was detected in CREB-bound chromatin indicating the co-occupancy of both SHP and CREB at these genes, and as a control, downregulation of CREB showed that the SHP occupancy in the CREB-bound chromatin was dependent on CREB (Fig 2D and Appendix Fig S6A). Consistent with the findings above that FGF19 inhibition of hepatic autophagy is likely independent of mTORC1 (Appendix Fig S2B–D), FGF19-mediated changes in occupancy of SHP, CREB, and CRTC2 were not affected by co-treatment with rapamycin in mice (Appendix Fig S5).

We next examined whether SHP and CREB directly interact. FGF19 treatment increased the interaction of endogenous SHP with CREB in Co-IP assays using liver extracts (Fig 2E). In GST-pull-down assays, SHP interacts through its N-terminal domain with the central transactivation KID domain of CREB (Fig 2F and Appendix Fig S6B). Interestingly, the CREB-interacting proteins, FXR (Seok *et al*, 2014) and CRTC2 (Koo *et al*, 2005; Dentin *et al*, 2007; Altarejos & Montminy, 2011), each interact with CREB through different domains that are distinct from the SHP-interaction domain (Fig 2F, top). Further, FGF19 treatment increased accumulation of SHP in the nucleus (Appendix Fig S6C), where CREB was located, enabling protein interaction. These results indicate that FGF19 treatment increases nuclear localization of SHP and that SHP interacts directly with CREB.

To further examine the functional interaction of SHP and CREB, reporter assays were performed using luciferase reporter constructs containing the *Tfeb, Atg3,* or *Atg7* promoter. Exogenous expression of SHP inhibited the reporter activation by CREB-CRTC2, and downregulation of SHP increased it (Fig 2G and Appendix Fig S6D). Consistent with these results, exogenous expression of CREB increased autophagy, and the increase was abolished by exogenous expression of SHP (Fig 2H). These results indicate that SHP inhibits the CREB transactivation of autophagy genes.

SHP epigenetically represses CREB-bound autophagy genes by recruiting LSD1

SHP represses expression of bile acid synthetic genes by recruiting histone-modifying enzymes, including LSD1, a key epigenetic factor that is recruited initially and required for subsequent repressive histone modifications, deacetylation of H3K9/14, and methylation of H3K9 (Kim *et al*, 2015b). LSD1 (also KDM1A) is a lysine-specific histone demethylase that represses genes by removing gene-activation histone marks, mono- or di-methylated H3K4 (Shi *et al*, 2004), but also activates genes by removing a gene-repression histone mark, methylated H3K9 (Metzger *et al*, 2005).

To determine whether LSD1 was involved in FGF19/SHP-mediated repression of autophagy, we first examined whether FGF19 treatment affects the interaction of SHP with LSD1. FGF19 treatment increased the interaction of endogenous SHP with LSD1 in liver extracts (Fig 3A). Further, FGF19 treatment increased LSD1 occupancy in SHP-bound chromatin at *Tfeb* and *Atg3* in re-ChIP assays and decreased histone H3K4-me2/3 and RNA polymerase II levels (Fig 3B). The increases in occupancy of LSD1 and decreases in the levels of histone H3K4-me2/3 at *Tfeb, Atg3*, and *Atg10* after FGF19 treatment were absent in $SHP^{-/-}$ mice (Fig 3C and Appendix Fig S7A), although protein levels of CREB, CRTC2, and LSD1 were similar in WT mice and $SHP^{-/-}$ mice (Appendix Fig S7B). These results indicate that FGF19 increases the interaction of SHP with LSD1 and that SHP recruits LSD1 to SHP-target autophagy genes.

In functional studies, exogenous expression of SHP inhibited CREB transactivation of *Tfeb-luc and Atg3-luc* reporters, and co-expression of LSD1 enhanced the inhibition, while downregulation of LSD1 reversed the SHP inhibition (Fig 3D, Appendix Fig S7C). Downregulation of SHP eliminated the effects of LSD1 on transcriptional activity of the promoters. Consistent with these results, downregulation of LSD1 increased, while expression of LSD1 decreased autophagy and these effects were absent if SHP was downregulated (Fig 3E). These results demonstrate that LSD1 inhibition of autophagy and autophagy gene expression is dependent on SHP.

LSD1 mediates epigenetic repression of SHP-target autophagy genes

FGF19 treatment or feeding of mice increased occupancy of LSD1, decreased occupancy of Pol II, decreased levels of gene-activation histone marks, H3K4-me2, H3K4-me3, and H3K9/14-Ac, and increased levels of a gene-repression mark, H3K9-me2, at SHP-target autophagy genes, *Tfeb, Atg3, and Atg7* (Fig 4A and B, Appendix Fig S7D and E). Downregulation of LSD1 (Appendix Fig S7F and G) partially or completely reversed these changes in histone modifications. In addition, FGF19- or feeding-mediated decreases in mRNA levels were attenuated in most SHP-target autophagy genes by downregulation of LSD1 in mice, and notably, basal expression of *Wipi1, Rb1cc1, and Uvrag* was substantially increased (Fig 4C and D). Further, FGF19 or feeding dramatically decreased the number of LC3 puncta in mouse liver, and downregulation of LSD1

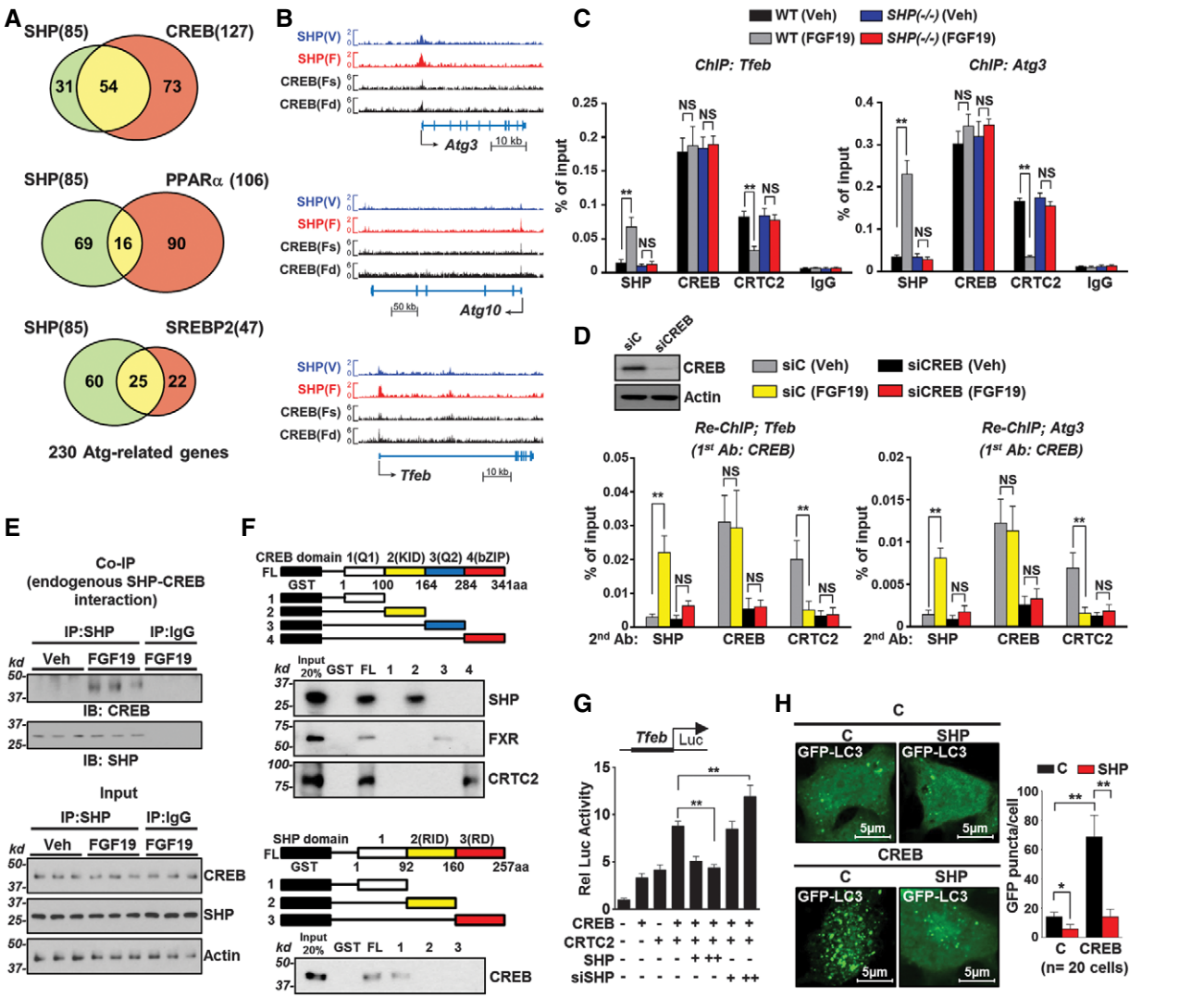

Figure 2. SHP represses CREB-target autophagy genes.

A Venn diagrams showing autophagy-related genes that contain binding peaks of SHP compared with those of activators of autophagy, CREB, PPARα, and SREBP-2, within 10 kb from the TSS.

B Display of autophagy-related genes with shared SHP and CREB binding peaks (UCSC genome browser).

C Mice were treated with FGF19 for 2 h, and three independent ChIP assays were done to detect occupancy of indicated proteins at *Tfeb* and *Atg3*.

D Hepatocytes were transfected with siRNA for CREB, and 48 h later, cells were treated with FGF19 for 2 h and re-ChIP was done with initial immunoprecipitation of CREB, followed by immunoprecipitation of SHP, CREB, and CRTC2 (n = 3).

E The effects of FGF19 treatment on the interaction of endogenous SHP with CREB in mouse liver nuclear extracts were detected by Co-IP (n = 3).

F Interactions of GST fusions of CREB with SHP, FXR, or CRTC2 or GST fusions of SHP with CREB were detected. Bound proteins were detected by IB. Domains of CREB and SHP fused to GST are shown above the IB blots.

G CREB, CRTC2, or SHP was expressed in Hepa1c1c7 cells or the cells were transfected with SHP siRNA as indicated, and luciferase reporter assays were done in triplicate (n = 4).

H GFP-LC3 and either SHP alone (top panels) or SHP and CREB (bottom panels) were expressed in Hepa1c1c7 cells. C indicates the control pcDNA3 vector. The cells were incubated in HBSS (2 h), and fluorescence was imaged by confocal microscopy. The average number of LC3-II puncta per cell is shown at the right (n = 20 cells).

Data information: Means ± SD are shown, and statistical significance was measured using (G) one- or (C, D, H) two-way ANOVA and Bonferroni post-test. *P < 0.05, **P < 0.01, and NS, statistically not significant.

substantially increased basal puncta numbers and partially reversed the decrease in the numbers of puncta after FGF19 or feeding from 80 to 50% (Fig 4E and F). FGF19 signaling assessed by p-ERK levels was normal in LSD1-downregulated mice (Appendix Fig S7H). These results indicate that LSD1 mediates the epigenetic repression of autophagy genes by SHP in a gene-selective manner.

SHP and LSD1 inhibit hepatic lipophagy

We next examined whether autophagy-mediated lipid catabolism, "lipophagy", is inhibited by SHP and LSD1. The co-localization of lipid droplets and autophagic GFP-LC3 puncta was increased by downregulation of SHP and LSD1 in Hepa1c1c7 cells (Fig 5A).

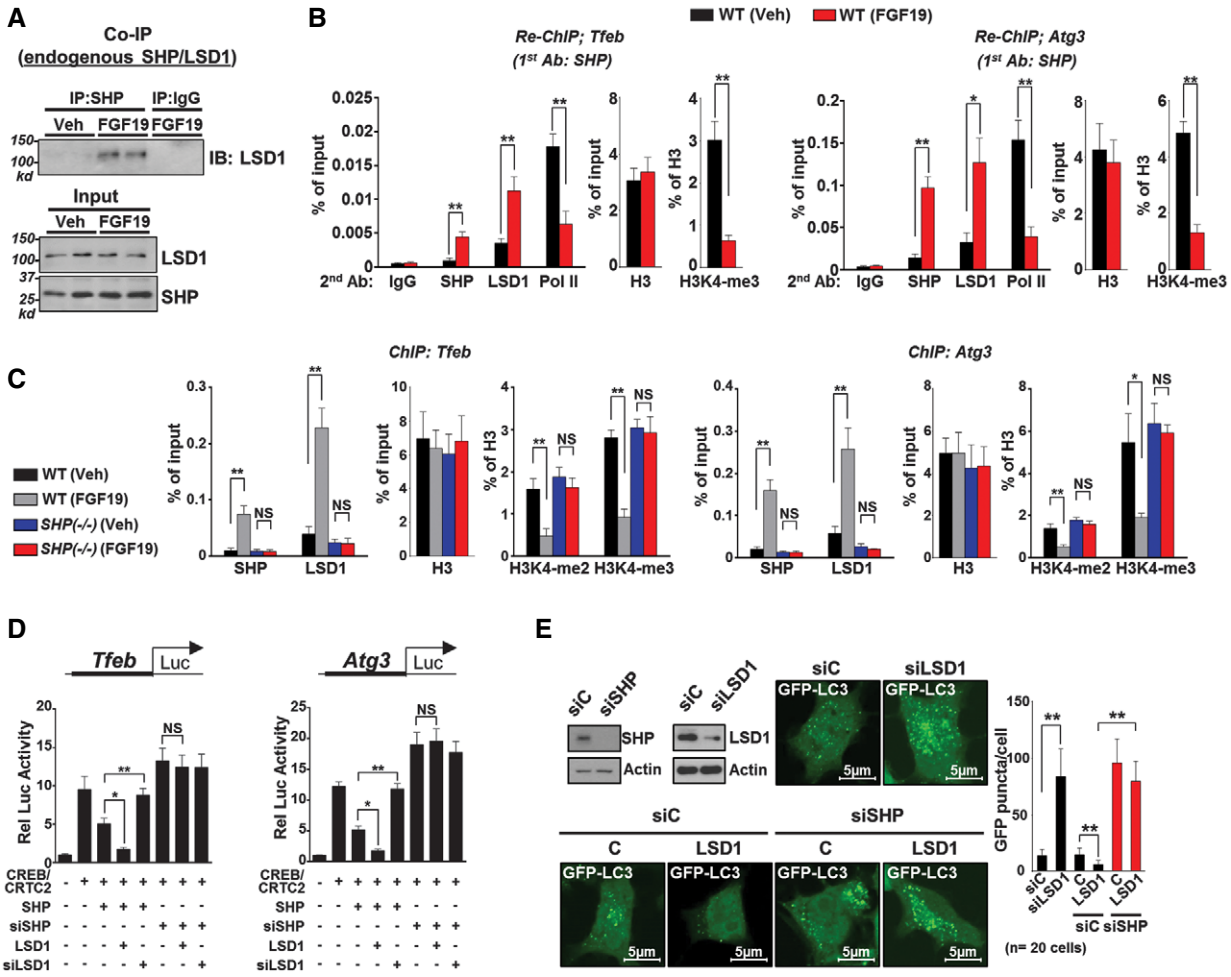

Figure 3. SHP represses CREB-target autophagy genes by recruiting LSD1.

A The interaction of SHP with LSD1 in mouse liver nuclear extracts was detected by Co-IP after FGF19 treatment.

B Mice were treated with FGF19, and re-ChIP assays were done with initial immunoprecipitation of SHP, followed by immunoprecipitation of the indicated proteins at the *Tfeb* and *Atg3* genes (n = 5).

C WT or *SHP*$^{-/-}$ mice were treated with FGF19 for 2 h, and liver ChIP assays (n = 3–5) were done to detect occupancy of indicated proteins and histone levels at *Tfeb* and *Atg3*.

D Hepa1c1c7 cells were transfected with expression plasmids and siRNAs as indicated, and reporter assays were done (n = 4).

E GFP-LC3 was expressed in Hepa1c1c7 cells, and the cells were transfected with control siRNA, siRNA for LSD1 or SHP, and LSD1 expression plasmids as indicated. C indicates the control pcDNA3 vector. The cells were incubated in HBSS (2 h), and fluorescence was imaged by confocal microscopy. The average number of LC3-II puncta per cell is shown at the right (n = 20 cells).

Data information: Means ± SD are shown, and statistical significance was measured using (B) Mann–Whitney test, (D) one- or (C, E) two-way ANOVA with the Bonferroni post-test, and (E) Student's t-test. *P < 0.05, **P < 0.01, and NS, statistically not significant.

However, these effects were significantly attenuated by downregulation of ATG7, a key component of the autophagosome. In electron microscopic studies in mouse liver, after downregulation of SHP or LSD1 in mice (Fig 5B), autophagic vesicles within lipid droplets were abundant, but were not observed in livers from control mice (Fig 5C and D). Further, lipid droplets detected by Oil Red O staining were reduced and serum and liver triglyceride levels were decreased in *SHP*$^{-/-}$ mice (Appendix Fig S8A–C). In WT mice, neutral lipid levels were increased in fasted mice but not in *SHP*$^{-/-}$ mice (Appendix Fig S8D), and fasting-induced accumulation of lipids was also modestly decreased in FGF15-KO mice (Appendix Fig S8E). These results demonstrate a role for SHP and LSD1 in inhibition of autophagy-mediated lipid mobilization.

ATGL is a major hepatic lipase that degrades triglycerides in lipid droplets and plays an important role in lipophagy (Singh *et al*, 2009; Ong *et al*, 2011; Singh & Cuervo, 2012). Binding peaks for SHP (Kim *et al*, 2015a) were detected at the promoter of *Atgl* (Fig 5E). FGF19 treatment increased occupancy of SHP and LSD1 at *Atgl* and decreased CRTC2 occupancy and levels of H3K4-me2/3 in WT mice, but not in *SHP*$^{-/-}$ mice, while CREB occupancy was not changed (Fig 5F, Appendix Fig S9A). Consistent with these results, FGF19 treatment (Fig 5G) or feeding (Appendix Fig S9B) repressed expression of *Atgl* in WT, but not in *SHP*$^{-/-}$ mice. Similar effects on

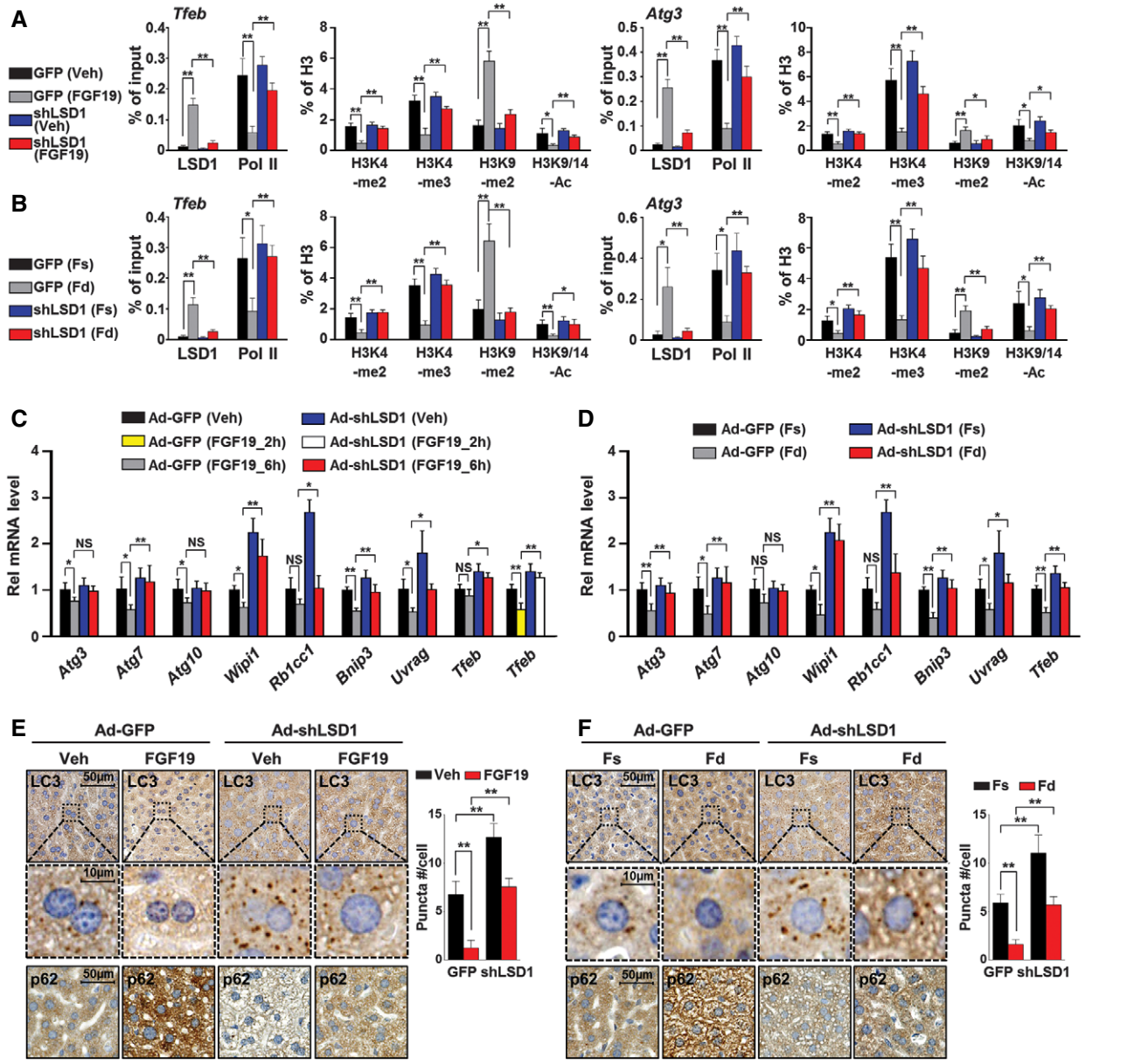

Figure 4. LSD1 mediates epigenetic repression of SHP-target autophagy genes.

Mice were injected via the tail vein with Ad-GFP or Ad-shRNA for LSD1, and 2 weeks later, mice were fasted for 12 h and then treated with FGF19 for 2 h (A, C, E) or refed for 6 h (B, D, F).

A, B ChIP assays (n = 3–4) for LSD1 and Pol II occupancy and histone modifications were done.

C, D The mRNA levels of indicated genes in liver were measured by qRT–PCR (n = 5 mice).

E, F Endogenous LC3 was detected by IHC in liver sections. Representative images of LC3-II puncta and the average number of puncta per cell are shown (n = 30 hepatocytes).

Data information: Means ± SD are shown, and statistical significance was measured using two-way ANOVA with the Bonferroni post-test. *P < 0.05, **P < 0.01, and NS, statistically not significant.

occupancy of factors and histone modifications and expression of *Atgl* were observed after liver-specific downregulation of LSD1 (Fig 5H and I, Appendix Fig S9C). These results suggest that SHP and LSD1 are required for FGF19- or feeding-mediated epigenetic repression of *Atgl* and provide additional evidence for a new function of SHP and LSD1 in hepatic lipophagy.

Both SHP and FXR inhibit autophagy after feeding in a mutually dependent manner

Bile acid-activated FXR inhibits hepatic autophagy in the fed-state by antagonizing CREB and PPARα activity (Lee *et al*, 2014; Seok *et al*, 2014), so it was important to determine the role of

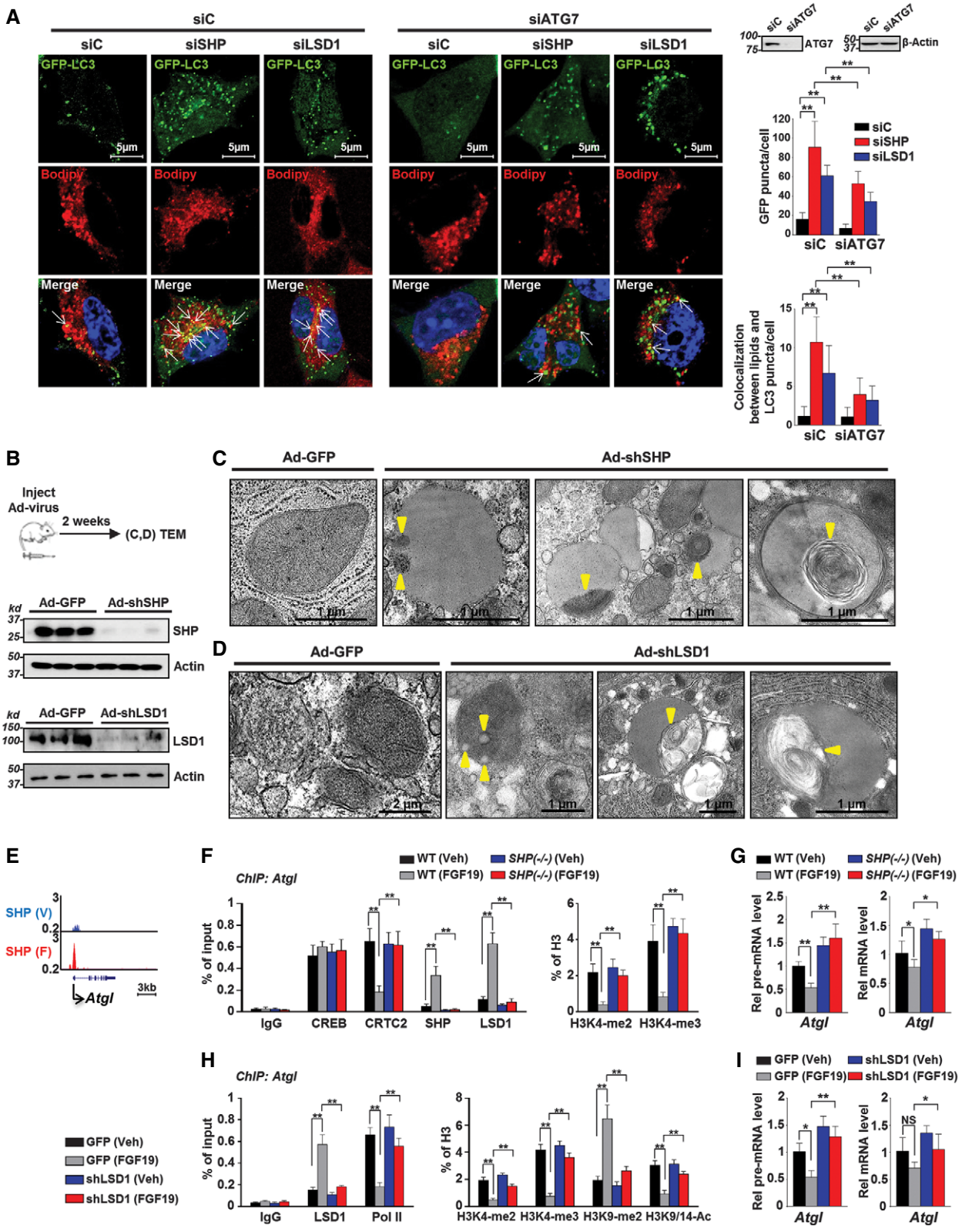

Figure 5.

FXR relative to SHP in regulating autophagy. We therefore compared the relative extent of feeding-mediated inhibition of autophagy by SHP and FXR *in vivo*. Feeding reduced the number of endogenous LC3 puncta in WT mice, and these effects were substantially blunted in both $SHP^{-/-}$ and $FXR^{-/-}$ mice (Fig 6A). Notably, basal numbers of LC3-II puncta were markedly

Figure 5. SHP and LSD1 inhibit hepatic lipophagy.

A GFP-LC3 (green) was expressed in Hepa1c1c7 cells, and the cells were transfected with control siRNA (*siC*) or siRNA for SHP, LSD1, or ATG7 as indicated. Cells were stained for lipid droplets with BODIPY (red) and imaged by confocal microscopy. Merged images are shown in the bottom row. Co-localization of LC3 and BODIPY is indicated by white arrows. The average number of fluorescent puncta per cell (right top, n = 20 cells) and the number of fluorescent puncta that co-localized with lipid staining (right bottom, n = 10 cells) are shown.

B Experimental outline. Mice were injected with adenoviral shRNA for SHP and LSD1 or control virus; 2 weeks later, hepatic SHP and LSD1 protein levels were detected by IB.

C, D Mice (n = 6) were injected via the tail vein with Ad-shRNA for SHP or LSD1 or control virus, and 2 weeks later, livers were collected for transmission electron microscopy analysis. Autophagy vesicles inside lipid droplets are indicated by yellow arrows.

E Normalized SHP binding peaks at the promoter region of *Atgl* gene are displayed (UCSC genome browser).

F WT or $SHP^{-/-}$ mice were treated with FGF19 for 2 h, and livers were collected for ChIP assays. Occupancy of indicated proteins at *Atgl* was detected by ChIP (n = 3–5).

G *Atgl* pre-mRNA and mRNA levels in vehicle- or FGF19-treated WT or $SHP^{-/-}$ mice were detected by qRT–PCR (n = 4–6).

H Mice were injected with Ad-GFP or Ad-shRNA for LSD1, and 2 weeks later, mice were fasted for 12 h and then treated with FGF19 for 2 h. ChIP assays (n = 3–4) for LSD1 and Pol II occupancy and histone modifications at *Atgl* gene were done.

I Mice were injected via the tail vein with Ad-GFP or Ad-shRNA for LSD1, and 2 weeks later, mice were fasted for 12 h and then treated with FGF19 for 6 h. Pre-mRNA and mRNA levels of *Atgl* gene in liver were measured by qRT–PCR (n = 5 mice).

Data information: Means ± SD are shown, and statistical significance was measured using two-way ANOVA with the Bonferroni post-test. *P < 0.05, **P < 0.01, and NS, statistically not significant.

increased in both mice, although they were more highly elevated in $SHP^{-/-}$ mice.

To further examine the relationship between FXR and SHP-FGF19 in repression of hepatic autophagy, FXR was activated with an FXR agonist GW4064 in $SHP^{-/-}$ mice, and conversely, $FXR^{-/-}$ mice were treated with FGF19. GW4064 treatment suppressed autophagy (Fig 6B) and autophagy-related gene expression (Fig 6C) as expected (Lee *et al*, 2014; Seok *et al*, 2014), and this inhibition was markedly diminished in $SHP^{-/-}$ mice. Conversely, basal numbers of LC3-II puncta and the basal ratio of LC3-II to LC3-I were increased in $FXR^{-/-}$ mice and were decreased after FGF19 treatment in both WT and $FXR^{-/-}$ mice, but were significantly higher after FGF19 treatment in $FXR^{-/-}$ mice compared to WT mice (Fig 6D and E). Notably, basal expression of SHP protein levels in mouse liver was decreased about 50% in $FXR^{-/-}$ mice (Appendix Fig S10A), and FGF19-mediated increases in SHP occupancy and decreases in Pol II occupancy at *Tfeb and Atg3* were partially blunted in $FXR^{-/-}$ mice (Appendix Fig S10B). These results suggest that both SHP and FXR inhibit hepatic autophagy upon feeding in a mutually dependent manner.

Temporal transcriptional repression of autophagy by SHP and FXR

Since both feeding-sensing nuclear receptors, FXR and FXR-induced SHP, repress autophagy, it was important to determine whether they act simultaneously or at different times after feeding. We therefore examined temporal changes after feeding in factor binding and histone modifications of CREB-target autophagy genes: (i) at promoter regions that contain only SHP peaks; (ii) in intron regions that contain only FXR peaks; or (iii) in promoter regions that contain both FXR and SHP peaks, based on ChIP-seq genomic analyses (Thomas *et al*, 2010; Lee *et al*, 2012; Kim *et al*, 2015a) (Appendix Fig S11, Appendix Table S6).

In *Uvrag* (Fig 7A, top, Appendix Fig S12A) and *Mapk8* (Appendix Fig S12B) with only a SHP peak at the promoter, feeding increased the occupancy of SHP, but not FXR, 4 and 8 h after feeding, while occupancy of RNA pol II was decreased. Occupancy of CREB was unchanged, but that of its coactivator CRCT2 was decreased at 4 and 8 h, while another CREB coactivator, p300 (Altarejos & Montminy, 2011), was unchanged. Occupancy of LSD1 and HDAC1/3 increased at 4 and 8 h, and levels of H3K4-me3 decreased as did those of H3K/9/14-Ac. Importantly, the feeding-induced recruitment of LSD1, decreased H3K4-me2 and H3K4-me3 levels, and increased H3K9-me2 levels were largely abolished in $SHP^{-/-}$ mice (Fig 7B, Appendix Fig S12C).

In *Atg4a* (Fig 7A, middle, Appendix Fig S12D) and *Atg9b* (Appendix Fig S12E) with only an FXR peak in the intron region, feeding for as short as 1 h increased the occupancy of FXR, but not SHP, and decreased the occupancy of RNA pol II and CRTC2. In sharp contrast to the genes with SHP binding sites, occupancy of LSD1 was not detected, and H3K4-me3 levels did not change. Remarkably, occupancy of p300 was dramatically decreased by 1 h, which presumably contributed to the decreased levels of H3K9/14-Ac. Importantly, the feeding-induced sharp dissociation of p300 was not observed in $FXR^{-/-}$ mice (Fig 7C).

In *Tfeb* (Fig 7A, bottom) and *Atg3, Atg7, and Atg10* (Appendix Fig S12F), with both SHP and FXR peaks in the promoters, essentially a composite of the results with the FXR-only and SHP-only binding sites was observed. FXR occupancy increased, CRTC2 and p300 occupancy decreased, and levels of H3K9/14-Ac decreased with time starting as early as 1 h after feeding. SHP and LSD1 occupancy increased and levels of H3K4-me3 decreased late at 4 and 8 h.

These results from extensive ChIP analyses demonstrate that postprandial transcriptional control of autophagy is temporally regulated by FXR and SHP, with FXR primarily acting in the early fed-state and SHP acting in the late fed-state. Both FXR and SHP cause dissociation of CRCT2, while FXR action is associated with dissociation of p300, and SHP recruits LSD1 histone demethylase, initiating an epigenetic cascade leading to gene repression.

Discussion

The present study identifies a new function for an FGF19-SHP-LSD1 axis in mediating postprandial epigenetic repression of hepatic autophagy. In response to feeding or FGF19 treatment, SHP recruits LSD1 to a subset of autophagy genes, which results in epigenetic

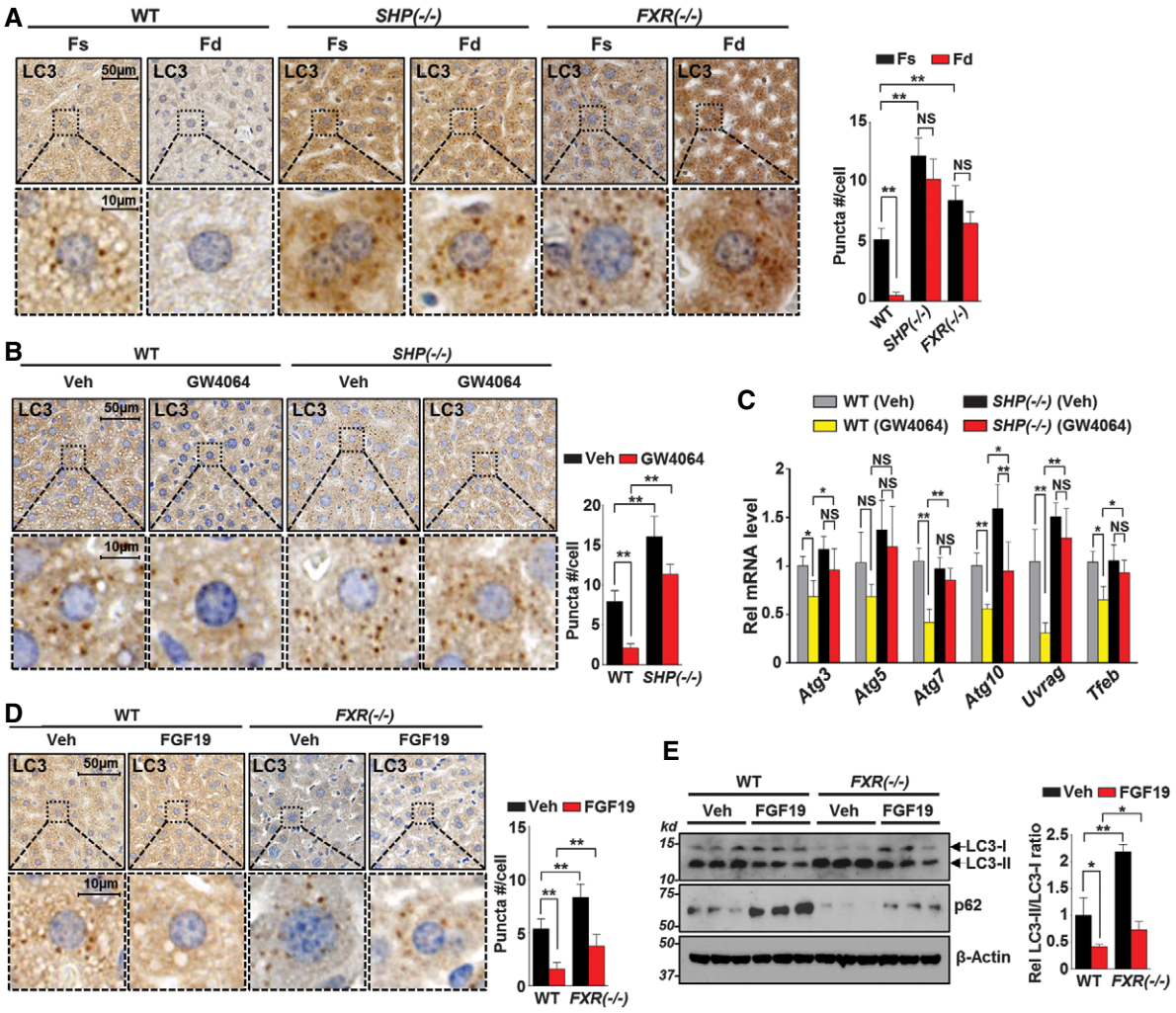

Figure 6. Both SHP and FXR inhibit hepatic autophagy after feeding in a mutually dependent manner.

A WT, *SHP*$^{-/-}$, or *FXR*$^{-/-}$ mice were fasted for 12 h (Fs) or refed for 6 h (Fd) after fasting, and LC3 in liver sections was detected by IHC. Representative images and the average numbers of LC3-II puncta per cell are shown (right, n = 30 hepatocytes).

B WT or *SHP*$^{-/-}$ mice were fasted for 12 h and then treated with GW4064 for 6 h, and endogenous LC3 was detected in liver sections by IHC. Representative images and the average number of LC3-II puncta per cell (right, n = 30 hepatocytes) are shown.

C mRNA levels of indicated genes were detected by qRT–PCR (n = 4–6).

D LC3 levels were detected by IHC analysis of liver sections from WT or *FXR*$^{-/-}$ mice treated with vehicle or FGF19. Representative images and the average number of LC3-II puncta per cell (right, n = 30 hepatocytes) are shown.

E LC3 levels in liver extracts from WT or *FXR*$^{-/-}$ mice treated with FGF19 were measured by IB. LC3-I and LC3-II intensities were quantified and the ratio of LC3-II to LC3-I was set to 1 for vehicle-treated WT mice (right, n = 3).

Data information: Means ± SD are shown, and statistical significance was measured using two-way ANOVA with the Bonferroni post-test. *P < 0.05, **P < 0.01, and NS, statistically not significant.

repression of these genes and decreased autophagic flux and macroautophagy, including lipophagy. Both FXR and SHP inhibit autophagy genes, but FXR acts predominantly early after feeding, while SHP acts relatively late, which effectively sustains postprandial repression of autophagy.

Despite the emerging importance of nuclear events in transcriptional regulation of autophagy by nutrient-sensing factors, epigenetic control linking metabolism and transcription is largely unexplored. LSD1 represses or activates its target genes by demethylating H3K4-me2 (Shi *et al*, 2004) or H3K9-me2 (Metzger *et al*, 2005), respectively, leading to context-dependent gene repression or activation. In the present study, we observed that in LSD1-downregulated mice, the demethylation of both H3K4-me2 and H3K4-me3 and subsequent repressive histone modifications after FGF19 treatment or feeding were attenuated. Notably, recruitment of LSD1 and the epigenetic repression cascade initiated by LSD1 binding were completely dependent on SHP. LSD1 acts, thus, as a key transcriptional partner of SHP in executing the epigenetic repression program for autophagy genes during feeding.

Regulation of autophagy after feeding is complex and involves temporal regulation by different mechanisms. Acute inhibition of autophagy by phosphorylation of nutrient-sensing kinases,

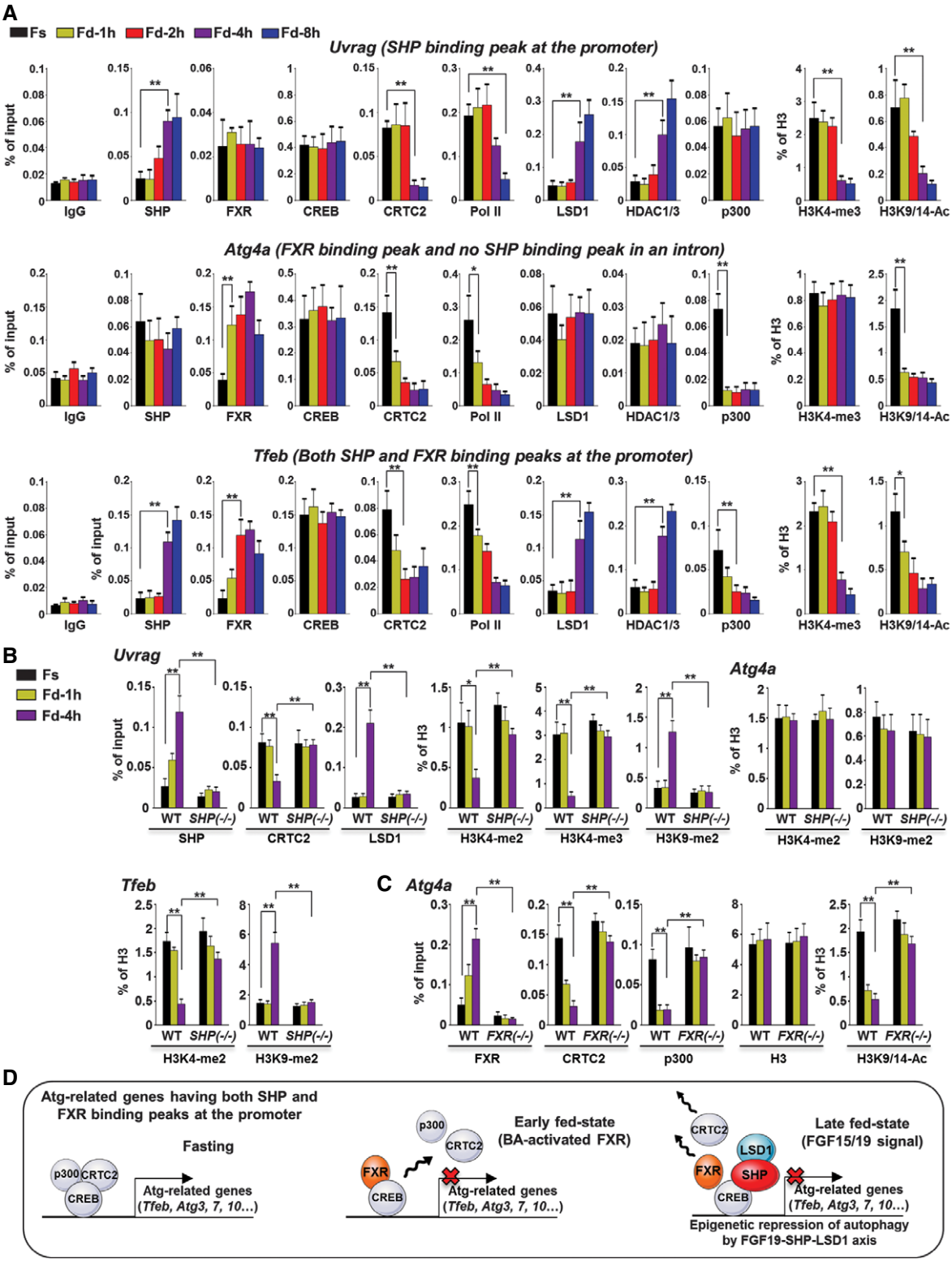

Figure 7.

including mTORC1, is well known (He & Klionsky, 2009; Kim *et al*, 2011). The current study reveals multiple transcriptionally regulated pathways that are initiated after feeding by the bile acid nuclear receptor FXR and further demonstrate the link between bile acid signaling and the autophagic pathway. Upon food intake, bile acid-activated FXR directly represses hepatic autophagy genes (Lee *et al*, 2014; Seok *et al*, 2014), but also induces the expression of SHP, LSD1 (Kim *et al*, 2015b), and FGF15/19 (Inagaki *et al*, 2005). Thus,

Figure 7. Occupancy of factors and modified histones at autophagy-related genes after feeding.

A Feeding time-course ChIP assays. Mice were fasted for 12 h and then fed for 1, 2, 4, or 8 h, and livers were collected for three independent ChIP assays. Occupancy of the indicated proteins and modified histones was detected by ChIP (top) at the promoter for *Uvrag*, which contains only a SHP binding peak, (middle) in an intron of *Atg4a*, which contains only an FXR binding peak, and (bottom) at the promoter of *Tfeb*, which contains both FXR and SHP peaks.

B WT or $SHP^{-/-}$ mice were fasted for 12 h (Fs) and then fed (Fd) for 1 or 4 h, and liver ChIP assays (n = 3) were done to detect occupancy of the indicated proteins and modified histones at *Uvrag*, *Atg4a*, and *Tfeb*.

C WT or $FXR^{-/-}$ mice were fasted for 12 h and then fed for 1 or 4 h and liver ChIP (n = 3) assays were done to detect occupancy of the indicated proteins and modified histones at *Atg4a*.

D Model of transcriptional regulation of Atg-related genes having both SHP and FXR peaks at the promoter. In the fasting state, the CREB-CRTC2 complex, together with p300, activates transcription of autophagy-related genes. In the early fed-state, bile acid-activated FXR directly interacts with CREB and disrupts the CREB-CRTC2 complex, which results in dissociation of p300 and CRTC2 from the complex and a decrease in H3K9/14-Ac levels. In response to FGF15/19 signaling in the late fed-state, SHP recruits LSD1 to a subset of CREB-bound autophagy genes, which results in epigenetic repression by eliminating the gene-activation histone marks, H3K4-me2/3, and in the subsequent repressive epigenetic cascade, including deacetylation of a gene-activation mark, H3K9/14-Ac, and methylation of a gene-repression mark, H3K9-me2.

Data information: Means ± SD are shown, and statistical significance was measured using (A) one- or (B, C) two-way ANOVA with the Bonferroni post-test. $*P < 0.05$, $**P < 0.01$. In (A), significance is indicated only for the first time point that is statistically significant.

direct FXR repression of autophagy would be expected to precede that by FXR-induced SHP, LSD1, and FGF15/19. Supporting this idea, in liver ChIP assays of mice fed for 1, 2, 4, or 8 h, FXR binding to selected autophagy genes was detected within 1 h of feeding, while SHP binding was delayed and increased at 4 h. Nevertheless, autophagy was blunted in both $FXR^{-/-}$ and $SHP^{-/-}$ mice, and FXR-mediated autophagy repression was reduced in $SHP^{-/-}$ mice and vice versa. Overall, interdependent sequential transcriptional repression by FXR and SHP effectively sustains postprandial repression of hepatic autophagy.

Transcriptional repression of autophagy occurs by different mechanisms for FXR and SHP, although both converge on CREB-mediated regulation (Fig 7D). In fasting, the CREB-CRTC2 complex, together with p300, activates transcription of autophagy-related genes. Bile acid-activated FXR binds to CREB and disrupts the CREB-CRTC2 complex (Seok *et al*, 2014) within 1 h after feeding, which is associated with a sharp decrease in p300 binding and decreased H3K9/14-Ac levels. LSD1 binding is not detected in autophagy genes in regions with only FXR binding sites. SHP binding, occurring at 4 h, results in recruitment of LSD1, and decreased levels of both H3K4-me2/3 and H3K9/14-Ac while p300 is not affected. Thus, both FXR and SHP cause dissociation of CRTC2 from CREB, while FXR also causes dissociation of p300, and SHP actively recruits LSD1 for epigenetic repression of autophagy genes.

After feeding, CRTC2 is phosphorylated, dissociates from the CREB-CRTC2 complex, and translocates to the cytoplasm (Koo *et al*, 2005; Dentin *et al*, 2007; Altarejos & Montminy, 2011). However, phosphorylation of CRTC2 does not appear to be sufficient for dissociation of CRTC2 from autophagy genes after feeding since the temporal dissociation of CRTC2 correlates closely with the early binding of FXR to its binding sites in autophagy genes and with the late binding of SHP at its binding sites (Fig 7). Nevertheless, inhibition of two tested genes, *Tfeb and Atg3,* was attenuated with the phosphor-defective CRTC2 S171A mutant that remains constitutively in the nucleus (Appendix Fig S13). Thus, both phosphorylation of CRTC2 and FXR or SHP binding at CREB-target autophagy genes likely contribute to the dissociation of CRTC2 from autophagy genes. Further studies will be required for clear understanding of potential cross-talk between acute nutrient-sensing kinase pathways and longer-term transcriptional pathways that control autophagy.

Lipids are stored or degraded depending on nutrient status. Multiple nutrient-sensing transcriptional factors, such as FXR, PPARα, CREB, and TFEB, link autophagy with lipid catabolism depending on nutrient availability (Settembre *et al*, 2013; Lee *et al*, 2014; Seok *et al*, 2014). TFEB is a master transcriptional activator of lipophagy and lysosomal gene networks, and its expression is regulated by these transcriptional factors, including TFEB itself, depending on nutrient status (Settembre *et al*, 2013). Recently, a histone arginine methyltransferase, CARM1, was identified as a global epigenetic coactivator of TFEB in transcriptional regulation of autophagy gene network (Shin *et al*, 2016). In the present study, we show that a SHP-LSD1 complex epigenetically represses expression of *Tfeb* and hepatic lipophagy, which would effectively sustain inhibition of unnecessary release of triglycerides from lipid droplets under nutrient-rich fed-state. Notably, we observed that SHP and LSD1 also epigenetically repress transcription of ATGL, a major hepatic lipase that mobilizes triglycerides in the lipid droplets (Ong *et al*, 2011), further supporting a new role for SHP-LSD1 in epigenetic repression of lipophagy.

In conclusion, we demonstrate that the postprandial FGF19-SHP-LSD1 axis epigenetically represses transcription of autophagy-related genes in the late fed-state and inhibits macroautophagy, including lipophagy. Epigenetics has emerged as an exciting area for drug development because epigenetic enzymes are often dysregulated in human diseases and they act in a gene-specific manner (Teperino *et al*, 2010; Lu & Thompson, 2012; Smith *et al*, 2012), as is the case with gene-selective repression of autophagy by SHP-LSD1 in this study. Both deficient and excessive autophagy are associated with human disease, including metabolic disorders, neurological disease, and cancer (Levine & Kroemer, 2008; Mizushima *et al*, 2008). The FGF19-SHP-LSD1 axis identified in this study may, thus, serve as a novel target for treatment of human diseases associated with autophagy dysfunction.

Materials and Methods

Reagents

Antibodies for SHP (sc-30169, H-160), FXR (sc-13063), CREB (sc-186), CRTC2 (sc-46272), RNA pol II (sc-9001), p300 (sc-585), HDAC1

(sc-7872), and HDAC3 (sc-11417) were purchased from Santa Cruz Biotechnology; for LSD1 (ab17721), H3 (ab1791), and H3K4-me3 (ab8580) from Abcam; for H3K4-me2 (#07-030), H3K9/K14-Ac (#06-599), and H3K9-me2 (#07-521) from Millipore; and for p-Ulk1(S757) (#14202), p-AMPK (#2535), AMPK (2532), p-ERK (#9101), ERK (#4695), p-S6K(T389) (#9234), S6K (#2708), β-actin (#4970), LC3 A/B (#4108), and p62 (#5114) from Cell Signaling. ON-TARGET*plus* siRNAs for SHP (M-062814), CREB (M-040959), LSD1 (M-065198), and Atg7 (M-049953) were purchased from Dharmacon, Inc. SHP antibody (sc-30169) was previously validated in WT and $SHP^{-/-}$ mice by ChIP (Kim *et al*, 2015a) and by IB and IHC in this study (Appendix Figs S8A and S10A).

Animal experiments

Male C57BL6, $SHP^{-/-}$, $FXR^{-/-}$, or $FGF15^{-/-}$ mice (8–12 weeks old, n = 3 to 6/group) were fasted for 12 h and injected iv with FGF19 (1 mg/kg) or ip with GW4064 (30 mg/kg in corn oil) at 9 a.m., and 2 or 6 h later, livers were collected. For feeding experiments, mice were fasted for 12 h (9:00 a.m. to 9:00 p.m.) and then refed for times as indicated. Animals were chosen at random for groups within the experiments, but no formal randomization methods were used and no blinding was done in group allocation or when assessing results. For adenoviral experiments, mice were injected via the tail vein with adenovirus ($0.5–1.0 \times 10^9$ active viral particles in 100 μl PBS), and 1–2 weeks later, the mice were sacrificed. For *in vivo* rapamycin experiments, C57BL6 mice (n = 3/group) were treated with vehicle, FGF19 (1 mg/kg, iv), rapamycin (1 mg/kg, ip), or both FGF19 and rapamycin for 2 h. All animal use and adenoviral protocols were approved by the Institutional Animal Care and Use and Biosafety Committees and were in accordance with National Institutes of Health guidelines.

Transmission electron microscopy (TEM)

TEM studies were done as previously described (Lee *et al*, 2014; Seok *et al*, 2014). Mouse liver samples were fixed in Karnovsky's fixative (phosphate-buffered 2% glutaraldehyde, 2.5% paraformaldehyde) and with 2% osmium tetroxide followed by the addition of 3% potassium ferricyanide for 30 min. After washing with water, samples were stained with uranyl acetate. The tissue was dehydrated with ethanol, acetonitrile was used as the transition fluid, and the sample was embedded in epoxy using the Epon substitute Lx112. Ultrathin sections were stained with uranyl acetate and lead citrate and imaged with a Hitachi H600 TEM.

IHC and IF

LC3 puncta in mouse liver or hepatic cells were detected as described previously (Seok *et al*, 2014). For Hepa1c1c7 cell studies, a GFP-LC3 plasmid and siRNA for the indicated genes (5–20 nM) were transfected, and 48 h later, cells were incubated in complete or HBSS media for 2 h. For IHC, LC3 and p62 proteins in mouse liver were detected using a HRP/DAB kit (Abcam, #Ab64261). Nuclei were stained with hematoxylin, and samples were imaged with a NanoZoomer (Hamamatsu). Liver tissue was frozen in OCT compound, sectioned, and stained with Oil Red O. SHP, CREB, and LSD1 were detected by IF as described previously (Seok *et al*, 2014).

Analysis of ChIP-seq data

Published ChIP-seq data for CREB (Everett *et al*, 2013), PPARα (Boergesen *et al*, 2012), SREBP-2 (Seo *et al*, 2011), and SHP (Kim *et al*, 2015a) were downloaded directly from the GEO database, and genomic locations of autophagy-related genes were retrieved from the refGene table (UCSC Genome Browser). Peaks were intersected with target genes except for CREB which we first converted peak coordinates from mouse sequence database mm8 to mm9 using liftOver. The detailed peak calling methods for each TF are listed (Appendix Table S6). We extracted ChIP-seq peaks within 10 kb of the TSS to the TES of autophagy genes. To identify CREB binding motifs on autophagy genes overlapping SHP peaks, FIMO (Grant *et al*, 2011) was used to search for CREB sites overlapping with SHP peaks (merged vehicle and FGF19 samples) using two known CREB motifs from the JASPAR 2014 database (MA0018.1 and MA0018.2) with $P > 0.001$.

Liver ChIP

ChIP and re-ChIP assays were performed as previously described (Kemper *et al*, 2009; Seok *et al*, 2014; Kim *et al*, 2015a). Briefly, livers were finely minced and incubated in PBS containing 1% formaldehyde for 10 min, and then, glycine was added. Cells were resuspended in hypotonic buffer and lysed by homogenization. Nuclei were pelleted and sonicated. The chromatin sample was precleared, and chromatin was immunoprecipitated using 1–1.5 μg of antibody or IgG as control. For re-ChIP assays, CREB and SHP were immunoprecipitated first and eluted by adding 10 mM DTT at 37°C for 30 min, and then, chromatin samples were diluted (20-fold) with buffer (20 mM Tris–HCl, pH 8.0, 150 mM NaCl, 2 mM EDTA, 1% Triton X-100) and re-precipitated. Chromatin was extensively washed and eluted, and the amounts of genomic DNA in the immunoprecipitates were determined by qPCR (primer sequences in Appendix Table S7). For analysis of modified histone levels by ChIP assay, the levels of modified histone H3 were normalized to total histone H3 levels.

Fluorescent detection of lipophagy

Hepa1c1c7 cells transfected with siRNAs and GFP-LC3 plasmid were analyzed as described (Seok *et al*, 2014). Lipids were stained with BODIPY and counterstained with DAPI. Green (GFP-LC3) and red (BODIPY) fluorescence was detected by confocal microscopy.

Hepatocyte experiments

Mouse hepatocytes were isolated by collagenase (0.8 mg/ml; Sigma-Aldrich Co.) perfusion. Hepatocytes were incubated with serum-free media and treated with vehicle or FGF19 (50 ng/ml) and with bafilomycin A_1 (100 nM). Levels of LC3 and p62 were detected by IB.

GST pull-down, Co-IP, and qRT–PCR

DNA fragments encoding CREB were inserted into the pGEX4T-1 at BamH1/Xho1 sites. Bacterially expressed and affinity-purified GST-fusion proteins were incubated with the reciprocal proteins that were synthesized by TNT (Promega, Inc.), and bound proteins were detected by IB. Co-IP assays were performed as previously described

(Kemper *et al*, 2009; Seok *et al*, 2014; Kim *et al*, 2015a). Briefly, liver extracts were prepared in Co-IP buffer (50 mM Tris, pH 8.0, 150 mM NaCl, 2 mM EDTA, 0.3% Nonidet P-40, 10% glycerol) and incubated with 1–2 μg of antibodies for 30 min, and 35 μl of 25% protein G-agarose was added. Two hours later, samples were washed with the Co-IP buffer and interacting proteins were detected by IB. Levels of mRNA were determined by qRT–PCR (primer sequences in Appendix Table S8) and normalized to those of 36B4.

Construction of *Atg3-luc*, *Atg7-luc*, and *Tfeb-luc*, and reporter assays

DNA fragments near *Atg3* (ch16: 45158843–45159230), *Atg7* (ch6: 114593018–114593483), and *Tfeb* (chr17: 47874210-47874643) that contained SHP peaks were amplified by PCR from mouse genomic DNA and cloned into the pGL3-basic-Luc vector. Luciferase reporter assays were done as described (Seok *et al*, 2014; Kim *et al*, 2015a). Luciferase activities were normalized to β-galactosidase activities.

Statistical analysis

GraphPad Prism 6 (GraphPad software version 6.01) was used for data analysis. Statistical significance was determined by Student's two-tailed *t*-test, Mann–Whitney test, or one- or two-way ANOVA with Bonferroni post-test for single or multiple comparisons as appropriate. Whenever relevant, the assumptions of normality were verified using the Shapiro–Wilk test, Kolmogorov–Smirnov test, and the D'agostino–Pearson omnibus test. P-values < 0.05 were considered as statistically significant.

Expanded View for this article is available online.

Acknowledgements
We thank Eric H. Xu for providing recombinant FGF19; Marc Montminy and Seung-Hoi Koo for CREB and CRTC2 expression plasmids and adenoviral vectors; and Kristina Schoonjans and Johan Auwerx for GST-SHP plasmids. We thank David Moore and Sayee Anakk for providing *SHP*$^{-/-}$ mice. EM studies were carried out in part in the Frederick Seitz Materials Research Laboratory Central Research Facilities, University of Illinois. This study was supported by an American Heart Association postdoctoral fellowship to SB (17POST33410223), by an American Heart Association scientist development award (16SDG27570006) to YK, and by grants from the National Institutes of Health (DK62777 and DK95842) and the American Diabetes Association (1-16-IBS-156) to JKK.

Author contributions
SB, BK, and JKK designed research; SB and Y-CK performed experiments; SB, Y-CK, BK, and JKK analyzed the data; BK, GG, and JS provided key materials; YZ and JM performed genomic analyses; and SB, BK, and JKK wrote the manuscript.

Conflict of interest
The authors declare that they have no conflict of interest.

References

Altarejos JY, Montminy M (2011) CREB and the CRTC co-activators: sensors for hormonal and metabolic signals. *Nat Rev Mol Cell Biol* 12: 141 – 151

Artal-Martinez de Narvajas A, Gomez TS, Zhang JS, Mann AO, Taoda Y, Gorman JA, Herreros-Villanueva M, Gress TM, Ellenrieder V, Bujanda L, Kim DH, Kozikowski AP, Koenig A, Billadeau DD (2013) Epigenetic regulation of autophagy by the methyltransferase G9a. *Mol Cell Biol* 33: 3983 – 3993

Boergesen M, Pedersen TA, Gross B, van Heeringen SJ, Hagenbeek D, Bindesboll C, Caron S, Lalloyer F, Steffensen KR, Nebb HI, Gustafsson JA, Stunnenberg HG, Staels B, Mandrup S (2012) Genome-wide profiling of liver X receptor, retinoid X receptor, and peroxisome proliferator-activated receptor alpha in mouse liver reveals extensive sharing of binding sites. *Mol Cell Biol* 32: 852 – 867

Dentin R, Liu Y, Koo SH, Hedrick S, Vargas T, Heredia J, Yates J III, Montminy M (2007) Insulin modulates gluconeogenesis by inhibition of the coactivator TORC2. *Nature* 449: 366 – 369

Egan DF, Shackelford DB, Mihaylova MM, Gelino S, Kohnz RA, Mair W, Vasquez DS, Joshi A, Gwinn DM, Taylor R, Asara JM, Fitzpatrick J, Dillin A, Viollet B, Kundu M, Hansen M, Shaw RJ (2011) Phosphorylation of ULK1 (hATG1) by AMP-activated protein kinase connects energy sensing to mitophagy. *Science* 331: 456 – 461

Everett LJ, Le Lay J, Lukovac S, Bernstein D, Steger DJ, Lazar MA, Kaestner KH (2013) Integrative genomic analysis of CREB defines a critical role for transcription factor networks in mediating the fed/fasted switch in liver. *BMC Genom* 14: 337

Fang S, Miao J, Xiang L, Ponugoti B, Treuter E, Kemper JK (2007) Coordinated recruitment of histone methyltransferase G9a and other chromatin-modifying enzymes in SHP-mediated regulation of hepatic bile acid metabolism. *Mol Cell Biol* 27: 1407 – 1424

Fullgrabe J, Lynch-Day MA, Heldring N, Li W, Struijk RB, Ma Q, Hermanson O, Rosenfeld MG, Klionsky DJ, Joseph B (2013) The histone H4 lysine 16 acetyltransferase hMOF regulates the outcome of autophagy. *Nature* 500: 468 – 471

Grant CE, Bailey TL, Noble WS (2011) FIMO: scanning for occurrences of a given motif. *Bioinformatics* 27: 1017 – 1018

He C, Klionsky DJ (2009) Regulation mechanisms and signaling pathways of autophagy. *Annu Rev Genet* 43: 67 – 93

Herzig S, Long F, Jhala US, Hedrick S, Quinn R, Bauer A, Rudolph D, Schutz G, Yoon C, Puigserver P, Spiegelman B, Montminy M (2001) CREB regulates hepatic gluconeogenesis through the coactivator PGC-1. *Nature* 413: 179 – 183

Inagaki T, Choi M, Moschetta A, Peng L, Cummins CL, McDonald JG, Luo G, Jones SA, Goodwin B, Richardson JA, Gerard RD, Repa JJ, Mangelsdorf DJ, Kliewer SA (2005) Fibroblast growth factor 15 functions as an enterohepatic signal to regulate bile acid homeostasis. *Cell Metab* 2: 217 – 225

Kemper J, Kim H, Miao J, Bhalla S, Bae Y (2004) Role of a mSin3A-Swi/Snf chromatin remodeling complex in the feedback repression of bile acid biosynthesis by SHP. *Mol Cell Biol* 24: 7707 – 7719

Kemper JK, Xiao Z, Ponugoti B, Miao J, Fang S, Kanamaluru D, Tsang S, Wu S, Chiang CM, Veenstra TD (2009) FXR acetylation is normally dynamically regulated by p300 and SIRT1 but constitutively elevated in metabolic disease states. *Cell Metab* 10: 392 – 404

Kerr TA, Saeki S, Schneider M, Schaefer K, Berdy S, Redder T, Shan B, Russell DW, Schwarz M (2002) Loss of nuclear receptor SHP impairs but does not eliminate negative feedback regulation of bile acid synthesis. *Dev Cell* 2: 713 – 720

Kim J, Kundu M, Viollet B, Guan KL (2011) AMPK and mTOR regulate autophagy through direct phosphorylation of Ulk1. *Nat Cell Biol* 13: 132 – 141

Kim YC, Byun S, Zhang Y, Seok S, Kemper B, Ma J, Kemper JK (2015a) Liver ChIP-seq analysis in FGF19-treated mice reveals SHP as a global transcriptional partner of SREBP-2. *Genome Biol* 16: 268

Kim YC, Fang S, Byun S, Seok S, Kemper B, Kemper JK (2015b) FXR-induced lysine-specific histone demethylase, LSD1, reduces hepatic bile acid levels and protects the liver against bile acid toxicity. *Hepatology* 62: 220 – 231

Kim DH, Kwon S, Byun S, Xiao Z, Park S, Wu SY, Chiang CM, Kemper B, Kemper JK (2016) Critical role of RanBP2-mediated SUMOylation of Small Heterodimer Partner in maintaining bile acid homeostasis. *Nat Commun* 7: 12179

Kir S, Beddow SA, Samuel VT, Miller P, Previs SF, Suino-Powell K, Xu HE, Shulman GI, Kliewer SA, Mangelsdorf DJ (2011) FGF19 as a postprandial, insulin-independent activator of hepatic protein and glycogen synthesis. *Science* 331: 1621 – 1624

Klionsky DJ (2007) Autophagy: from phenomenology to molecular understanding in less than a decade. *Nat Rev Mol Cell Biol* 8: 931 – 937

Kong B, Huang J, Zhu Y, Li G, Williams J, Shen S, Aleksunes LM, Richardson JR, Apte U, Rudnick DA, Guo GL (2014) Fibroblast growth factor 15 deficiency impairs liver regeneration in mice. *Am J Physiol Gastrointest Liver Physiol* 306: G893 – G902

Koo SH, Flechner L, Qi L, Zhang X, Screaton RA, Jeffries S, Hedrick S, Xu W, Boussouar F, Brindle P, Takemori H, Montminy M (2005) The CREB coactivator TORC2 is a key regulator of fasting glucose metabolism. *Nature* 437: 1109 – 1111

Lee J, Seok SM, Yu P, Kim K, Smith Z, Rivas-Astroza M, Zhong S, Kemper JK (2012) Genomic analysis of hepatic Farnesoid X Receptor (FXR) binding sites reveals altered binding in obesity and direct gene repression by FXR. *Hepatology* 56: 108 – 117

Lee JM, Wagner M, Xiao R, Kim KH, Feng D, Lazar MA, Moore DD (2014) Nutrient-sensing nuclear receptors coordinate autophagy. *Nature* 516: 112 – 115

Levine B, Kroemer G (2008) Autophagy in the pathogenesis of disease. *Cell* 132: 27 – 42

Lu C, Thompson CB (2012) Metabolic regulation of epigenetics. *Cell Metab* 16: 9 – 17

Lundasen T, Galman C, Angelin B, Rudling M (2006) Circulating intestinal fibroblast growth factor 19 has a pronounced diurnal variation and modulates hepatic bile acid synthesis in man. *J Intern Med* 260: 530 – 536

Metzger E, Wissmann M, Yin N, Muller JM, Schneider R, Peters AH, Gunther T, Buettner R, Schule R (2005) LSD1 demethylates repressive histone marks to promote androgen-receptor-dependent transcription. *Nature* 437: 436 – 439

Mizushima N, Levine B, Cuervo AM, Klionsky DJ (2008) Autophagy fights disease through cellular self-digestion. *Nature* 451: 1069 – 1075

Mizushima N (2009) Physiological functions of autophagy. *Curr Top Microbiol Immunol* 335: 71 – 84

Mizushima N, Yoshimori T, Levine B (2010) Methods in mammalian autophagy research. *Cell* 140: 313 – 326

Ong KT, Mashek MT, Bu SY, Greenberg AS, Mashek DG (2011) Adipose triglyceride lipase is a major hepatic lipase that regulates triacylglycerol turnover and fatty acid signaling and partitioning. *Hepatology* 53: 116 – 126

Rabinowitz JD, White E (2010) Autophagy and metabolism. *Science* 330: 1344 – 1348

Seo YK, Jeon TI, Chong HK, Biesinger J, Xie X, Osborne TF (2011) Genome-wide localization of SREBP-2 in hepatic chromatin predicts a role in autophagy. *Cell Metab* 13: 367 – 375

Seok S, Fu T, Choi SE, Li Y, Zhu R, Kumar S, Sun X, Yoon G, Kang Y, Zhong W, Ma J, Kemper B, Kemper JK (2014) Transcriptional regulation of autophagy by an FXR-CREB axis. *Nature* 516: 108 – 111

Settembre C, De Cegli R, Mansueto G, Saha PK, Vetrini F, Visvikis O, Huynh T, Carissimo A, Palmer D, Jurgen Klisch T, Wollenberg AC, Di Bernardo D, Chan L, Irazoqui JE, Ballabio A (2013) TFEB controls cellular lipid metabolism through a starvation-induced autoregulatory loop. *Nat Cell Biol* 15: 647 – 658

Shi Y, Lan F, Matson C, Mulligan P, Whetstine JR, Cole PA, Casero RA, Shi Y (2004) Histone demethylation mediated by the nuclear amine oxidase homolog LSD1. *Cell* 119: 941 – 953

Shin HJ, Kim H, Oh S, Lee JG, Kee M, Ko HJ, Kweon MN, Won KJ, Baek SH (2016) AMPK-SKP2-CARM1 signalling cascade in transcriptional regulation of autophagy. *Nature* 534: 553 – 557

Singh R, Kaushik S, Wang Y, Xiang Y, Novak I, Komatsu M, Tanaka K, Cuervo AM, Czaja MJ (2009) Autophagy regulates lipid metabolism. *Nature* 458: 1131 – 1135

Singh R, Cuervo AM (2012) Lipophagy: connecting autophagy and lipid metabolism. *Int J Cell Biol* 2012: 282041

Smith Z, Ryerson D, Kemper JK (2012) Epigenomic regulation of bile acid metabolism: emerging role of transcriptional cofactors. *Mol Cell Endocrinol* 368: 59 – 70

Teperino R, Schoonjans K, Auwerx J (2010) Histone methyl transferases and demethylases; can they link metabolism and transcription? *Cell Metab* 12: 321 – 327

Thomas AM, Hart SN, Kong B, Fang J, Zhong XB, Guo GL (2010) Genome-wide tissue-specific farnesoid X receptor binding in mouse liver and intestine. *Hepatology* 51: 1410 – 1419

Wang L, Lee Y, Bundman D, Han Y, Thevananther S, Kim C, Chua S, Wei P, Heyman R, Karin M, Moore D (2002) Redundant pathways for negative feedback regulation of bile acid production. *Dev Cell* 2: 721 – 731